Estimating Glioblastoma Biophysical Growth Parameters Using Deep Learning Regression

Sarthak Pati[1,2,6], Vaibhav Sharma[3], Heena Aslam[3], Siddhesh P. Thakur[1,2,6], Hamed Akbari[1,2], Andreas Mang[4], Shashank Subramanian[5], George Biros[5], Christos Davatzikos[1,2], and Spyridon Bakas[1,2,6(✉)]

[1] Center for Biomedical Image Computing and Analytics, University of Pennsylvania, Philadelphia, PA, USA
sbakas@upenn.edu
[2] Department of Radiology, Perelman School of Medicine, University of Pennsylvania, Philadelphia, PA, USA
[3] Department of Electrical and Electronics Engineering, Aligarh Muslim University, Aligarh, Uttar Pradesh, India
[4] Department of Mathematics, University of Houston, Houston, TX, USA
[5] Oden Institute of Computational Engineering and Sciences, The University of Texas at Austin, Austin, TX, USA
[6] Department of Pathology and Laboratory Medicine, Perelman School of Medicine, University of Pennsylvania, Philadelphia, PA, USA

Abstract. Glioblastoma (***GBM***) is arguably the most aggressive, infiltrative, and heterogeneous type of adult brain tumor. Biophysical modeling of GBM growth has contributed to more informed clinical decision-making. However, deploying a biophysical model to a clinical environment is challenging since underlying computations are quite expensive and can take several hours using existing technologies. Here we present a scheme to accelerate the computation. In particular, we present a deep learning (***DL***)-based logistic regression model to estimate the GBM's biophysical growth in seconds. This growth is defined by three tumor-specific parameters: 1) a diffusion coefficient in white matter (***Dw***), which prescribes the rate of infiltration of tumor cells in white matter, 2) a mass-effect parameter (***Mp***), which defines the average tumor expansion, and 3) the estimated time (***T***) in number of days that the tumor has been growing. Preoperative structural multi-parametric MRI (***mpMRI***) scans from $n = 135$ subjects of the TCGA-GBM imaging collection are used to quantitatively evaluate our approach. We consider the mpMRI intensities within the region defined by the abnormal FLAIR signal envelope for training one DL model for each of the tumor-specific growth parameters. We train and validate the DL-based predictions against parameters derived from biophysical inversion models. The average Pearson correlation coefficients between our DL-based estimations and the biophysical parameters are 0.85 for Dw, 0.90 for Mp, and 0.94 for T, respectively.

C. Davatzikos and S. Bakas—Equally contributing senior author.

A. Crimi and S. Bakas (Eds.): BrainLes 2020, LNCS 12658, pp. 157–167, 2021.
https://doi.org/10.1007/978-3-030-72084-1_15

This study unlocks the power of tumor-specific parameters from biophysical tumor growth estimation. It paves the way towards their clinical translation and opens the door for leveraging advanced radiomic descriptors in future studies by means of a significantly faster parameter reconstruction compared to biophysical growth modeling approaches.

Keywords: Deep learning · Regression · Glioblastoma · Brain tumor · Biophysical growth model

1 Introduction

Glioblastoma (***GBM***), being the most common, aggressive, and infiltrative adult brain tumor, has unfavorable prognosis [1,2]. Recent advances in clinical GBM care has not made a huge difference to patient prospects [3]. The highly infiltrative nature of GBM render its recurrence essentially a guaranteed process [4,5] and its management varies drastically on a case-by-case basis. Integration of computational imaging, biophysical modeling, and machine learning has the potential to provide valuable tools to aid clinical diagnosis and decision making in a consistent and reproducible way [6], and by that possibly dramatically improve treatment planning for patients diagnosed with GBM [7–17].

In particular, biophysical modelling has the potential to become an indispensable tool to provide additional insights into GBM progression and development, and hence improve clinical decision making resulting in further improving quality of life for patients [6]. For example, in Fig. 1, the growth characteristics of the tumor would help stratifying the tumor into "proliferating" (tumor predominantly growing by hyperplasia and hypertrophy that push surrounding normal tissues), "infiltrating" (tumor predominantly growing by invasion and replacing surrounding tissues without mass effects) or "necrotic" (tumor is predominantly stagnant). Previous works [6,18–28] have used rigorous mathematical modelling to automatically estimate parameters that define the physical characteristics of tumor progression. In the present work, we consider the following main parameters:

1. *Diffusion coefficient in white matter (Dw).* This parameter, also termed as *diffusivity*, controls the rate at which tumor cells infiltrate white matter [29].
2. *Mass-effect parameter (Mp).* This parameter captures the mechanical deformation of the brain parenchyma caused as a function of the tumor growth [30], and defines the average tumor expansion. Clinically, this parameter quantifies how much the surrounding tissues deform because of the force exerted by the tumor's expansion.
3. *Estimated time (T).* This parameter defines the number of days the tumor has been expanding [31].

In this study, we propose a deep learning (***'DL'***) based regression model (see Sect. 2.3) to glean multi-parametric insight into the data by *training* on the parameter values extracted using Boosted GLioma Image SegmenTation

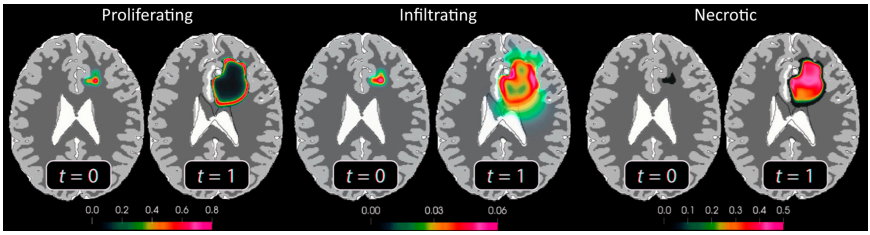

Fig. 1. Tumor proliferation across two time-points. These figures showcase the different types of clinical diagnoses that arise from the considered tumor growth parameters.

and Registration (GLISTRboost[1]) , which can then be used to approximate the aforementioned parameters during the *inference* phase. Our results (Sect. 3) show that this approach compares favorably to the current state-of-the-art, and is significantly more efficient during inference. This reduction in execution time is a critical for deploying our methodology in a clinical setting.

2 Methods

2.1 Data

The Cancer Imaging Archive (TCIA) [32] has released The Cancer Genome Atlas Glioblastoma Multiforme (TCGA-GBM) collection [33], which contains clinically-acquired multi-parametric MRI (mpMRI) scans for all patients of the collection. TCIA Analysis Results repository also offers a curated version of this collection, extended by corresponding segmentation labels and imaging features for all ($n = 135$) the pre-operative structural scans of the TCGA-GBM collection [34]. These mpMRI explicitly refer to native T1-weighted (T1) and post-contrast T1-weighted (T1Gd) scans, T2-weighted (T2), and T2 Fluid-Attenuated Inversion Recovery (FLAIR) scans. Furthermore, the included imaging features, also contain estimates for the parameters of interest, namely, Dw, Mp, and T. We use these parameter estimates along with the image intensities present in the abnormal FLAIR signal envelope to train the proposed DL model.

2.2 Pre-processing

To guarantee the homogeneity of the dataset, we applied the same pre-processing pipeline across all mpMRI scans. All the raw DICOM scans obtained from TCIA are converted to the NIfTI [35] file format. Subsequently, we followed the protocol for pre-processing as defined in the International Brain Tumor Segmentation (BraTS) challenge [36–38]. Specifically, each patient's T1Gd scan was rigidly registered to a common anatomical atlas of $240 \times 240 \times 155$ image size, and resampled to an isotropic resolution of $1\,\text{mm}^3$ [39]. The remaining scans of each patient

[1] https://www.med.upenn.edu/cbica/sbia/glistrboost.html.

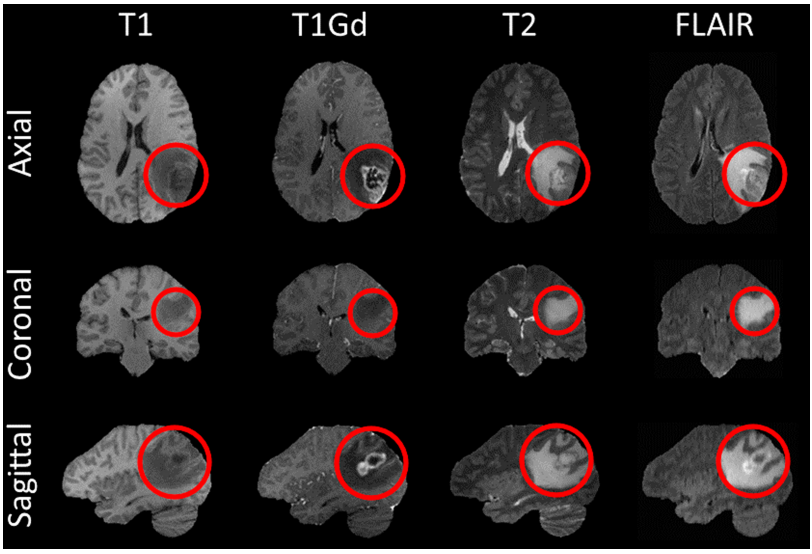

Fig. 2. Images of pipeline described in Sect. 2.2. The region of pathology used to train the DL model is highlighted using a red circle. (Color figure online)

(T1, T2, FLAIR) were subsequently rigidly co-registered to the same patient's resampled T1Gd scan. All the registrations were done using Greedy ([2]) [40] - a CPU-based C++ implementation of the greedy diffeomorphic registration algorithm and is integrated into the ITK-SNAP ([3]) segmentation software [41], as well as the Cancer Imaging Phenomics Toolkit (CaPTk ([4])) [42–44]. Following registration to a common anatomical atlas, and resampling to an isotropic resolution of $1mm^3$, we perform instance-level normalization, where the intensity of each modality of each individual subject is normalized to zero mean and unit variance. This process is also known as Z-scoring, after which we performed skull stripping using BrainMaGe ([5]) [45] (see Fig. 2). We use the z-score normalized images during the downstream analysis.

All intensities of the whole tumor, defined by the whole abnormal FLAIR signal envelope, for each of the mpMRI modalities are concatenated in a 1D vector. This results in a stacked 2D matrix, where the number of rows define the intensities picked from all voxel included in the whole tumor region, and the number of columns equates to the number of the input mpMRI modalities, i.e., 4. This 2D matrix forms the data of each patient used in our proposed approach. This process is done over the entire dataset and, with the exception of 20% of

[2] https://github.com/pyushkevich/greedy.
[3] http://www.itksnap.org.
[4] https://www.cbica.upenn.edu/captk.
[5] https://github.com/CBICA/BrainMaGe/.

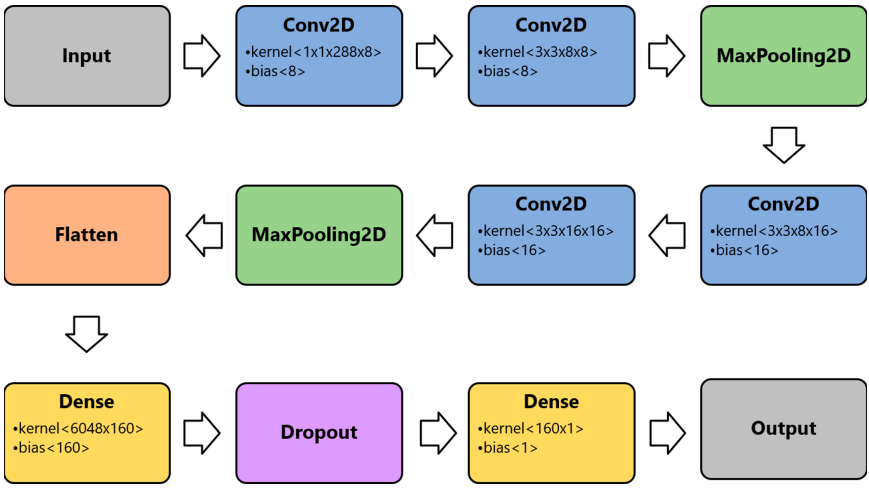

Fig. 3. The base model used to train for all 3 parameters.

the data held out for final performance evaluation, forms the complete *training input data*.

2.3 Network Topology

Once the *training input data* is constructed, we train one 2D DL model for each of the three parameters that are to be predicted. Each DL model consisted of two sets of convolution layers, each set followed by a single max-pooling layer. After feature reduction using the convolution/max-pooling layers, a fully connected flatten layer is used to flatten the output from the last max pooling layer. The flatten layer is followed by a fully connected dense layer having 160 nodes (which ensures a fixed number of inputs going into the final dense layer, regardless of the number of intensities) and followed by a 20% dropout (see Fig. 3). The model is trained using an adaptive gradient algorithm with an initial learning rate of 1E–2, and the model minimization metric used is normalized root mean squared error (NRMS), which is defined as follows:

$$NRMS = \sqrt{\frac{1}{N}\sum_{i=1}^{N}(x_i - y_i)}, \tag{1}$$

where x_i, y_i denotes the original and predicted observations indexed with i, respectively, and N represents the total number of samples.

2.4 Experimental Design

The current state-of-the-art approaches for personalized brain tumor modeling and parameter estimation consider optimization formulations with multiple, tightly coupled partial differential equations as constraints [6]. These types of

approaches pose formidable computational and mathematical challenges [6]. Our hypothesis for this study is that a regression-based machine learning technique would be able to capture these parameters using the outputs of a widely-accepted computational method for biophysical inversion, GLISTRboost [18,19], whose results are presented in the dataset provided by TCIA, as described in Sect. 2.1.

In this study, the region of pathology was obtained using the FLAIR abnormal signal, which defines the whole tumor, i.e., the peritumoral edematous/invaded tissue combined with the enhancing and the necrotic parts of the tumor. The image intensities of all mpMRI scans from this region, along with the original parameter estimations from GLISTRboost, are used as the training data. Three separate models, one for each parameter that needs to be modelled and each of which has the network topology defined in Sect. 2.3, was trained using a 10-fold cross validation scheme [46]. We utilized a nested cross-validation based training i) in favor of reproducibility, ii) while attempting to avoid over-fitting to the training data, and iii) to tune the network hyper-parameters in a more robust manner.

2.5 Evaluation Metric

Following the literature on similar predictive modelling and classification tasks [47,48], we have used the Pearson's correlation coefficient (r_p) [49] to evaluate the efficacy of the network. These measures are defined as follows:

$$r_p = \frac{\sum_{i=1}^{N}(x_i - \bar{x})(y_i - \bar{y})}{\sqrt{\sum_{i=1}^{N}(x_i - \bar{x})^2}\sqrt{\sum_{i=1}^{N}(y_i - \bar{y})^2}}, \tag{2}$$

where x_i, y_i denotes the original and predicted observations indexed with i, respectively, N represents the total number of observations, and $\bar{x}, \bar{y}$ are the sample means for the original and predicted values, respectively.

3 Results

Following the experimental design described in Sect. 2.4, we used the training data of the fold with the best accuracy (defined as the lowest NRMS loss) to validate against a hold-out set of $n = 20$ subjects. Notably this hold out set was excluded from the cross-validated training phase. We estimated the Pearson's correlation coefficient between the original and predicted values. The experimental results for all the 10 folds (see Fig. 4) show that the DL models were able to approximate the parameters reasonably well.

From Fig. 4, it is evident that the model's performance is best for Mp, with the best correlation score of $r_p = 0.99$. The median correlation scores for Mp and Dw are $r_p = 0.89$, and $r_p = 0.889$, respectively. In terms of stability, the model that predicts T performs best, with a median correlation score of $r_p = 0.92$. This highlights the need for more rigorous validation with increased amount of diverse datasets and possibly using more sophisticated modelling techniques, such as the one described in [50].

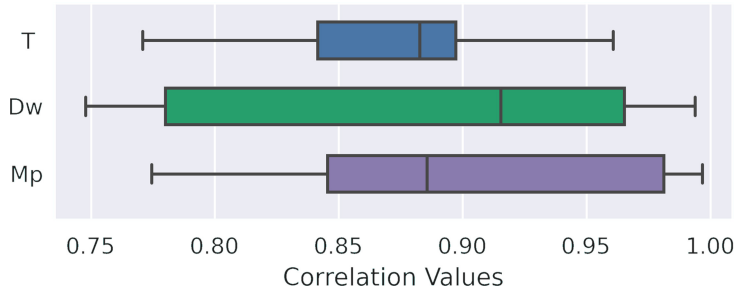

Fig. 4. Pearson's correlation coefficient for original and predicted values for the growth parameters under consideration across 10 training folds.

4 Discussion

This study compares the outputs from an existing mathematically rigorous formulation of a biophysical modelling technique [19] provided by TCIA [32–34] with that of the proposed DL model, trained solely on image intensities and those pre-existing estimates of tumor growth parameters. Using a 2D convolution based architecture for the DL network, combined with a normalized mean squared error loss (see Sect. 2.3 for details), and intensity values from the pathological region of the dataset, we were able to get favorable results for data not seen by the model during training, as show in Sect. 3.

The most notable difference was that for the inference phase for predicting the growth parameters, where the DL-based method took about 15–30 s on a GPU (NVIDIA Titan Xp), and 2–5 min when executed on a CPU architecture (Intel i7-8700K). This is in contrast to the mathematical formulation (GLISTRboost [18]), which would take about 5 h on the same CPU. This significant reduction in run-time renders such methods for parameter estimation potentially translatable to clinical applications.

The results presented in this explorative study show that the proposed framework yields a good accompanying tool along with sophisticated mathematical modelling techniques, where the latter is used to generate the training data. We note that our framework is generic; introducing more complicated (realistic) mathematical models of tumor progression alongside with efficient numerical methods for their solution into the training phase forms the basis of our current research. Additionally, we note that this method is limited in capability and confined by the input training data, and more work is needed to ensure further analysis of the generalizability of the proposed method when compared with biophysical tumor growth modelling techniques.

We envision an integrated computational framework that augments clinical imaging data in a consistent and reproducible way by estimating tumor growth model parameters for individual patients, without the burden of extreme computational footprint, with the potential to be clinically translated and hence aid clinical decision making, towards ultimately improving clinical outcome. Towards

this end, future extensions of this work involve including texture characteristics and spatial information to the network, as well as using a fully-connected 3D architecture, while studying the effects of these parameters for clinically-relevant outcomes such as survival prediction.

Acknowledgments. Research reported in this publication was partly supported by the National Institutes of Health (NIH) under award number NIH/NCI:U01CA242871, NIH/NINDS:R01NS042645, NIH/NCI:U24CA189523. The content of this publication is solely the responsibility of the authors and does not represent the official views of the NIH.

References

1. Ostrom, Q.T., Rubin, J.B., Lathia, J.D., Berens, M.E., Barnholtz-Sloan, J.S.: Females have the survival advantage in glioblastoma. Neuro Oncol. **20**(4), 576 (2018)
2. Herrlinger, U., et al.: Lomustine-temozolomide combination therapy versus standard temozolomide therapy in patients with newly diagnosed glioblastoma with methylated MGMT promoter (CeTeG/NOA-09): a randomised, open-label, phase 3 trial. The lancet **393**(10172), 678–688 (2019)
3. Hou, L.C., Veeravagu, A., Hsu, A.R., Victor, C.: Recurrent glioblastoma multiforme: a review of natural history and management options. Neurosurg. Focus **20**(4), E3 (2006)
4. Akbari, H., et al.: Imaging surrogates of infiltration obtained via multiparametric imaging pattern analysis predict subsequent location of recurrence of glioblastoma. Neurosurgery **78**(4), 572–580 (2016)
5. Fathi Kazerooni, A., et al.: Cancer imaging phenomics via CaPTk: multi-institutional prediction of progression-free survival and pattern of recurrence in glioblastoma. JCO Clin. Cancer Inf. **4**, 234–244 (2020)
6. Mang, A., Bakas, S., Subramanian, S., Davatzikos, C., Biros, G.: Integrated biophysical modeling and image analysis: application to neuro-oncology. Ann. Rev. Biomed. Eng. **22**, 309–341 (2020)
7. Gutman, D.A., et al.: MR imaging predictors of molecular profile and survival: multi-institutional study of the TCGA glioblastoma data set. Radiology **267**(2), 560–569 (2013)
8. Gevaert, O., et al.: Glioblastoma multiforme: exploratory radiogenomic analysis by using quantitative image features. Radiology **273**(1), 168–174 (2014)
9. Jain, R., et al.: Outcome prediction in patients with glioblastoma by using imaging, clinical, and genomic biomarkers: focus on the nonenhancing component of the tumor. Radiology **272**(2), 484–493 (2014)
10. Aerts, H.J.: The potential of radiomic-based phenotyping in precision medicine: a review. JAMA Oncol. **2**(12), 1636–1642 (2016)
11. Bilello, M., et al.: Population-based MRI atlases of spatial distribution are specific to patient and tumor characteristics in glioblastoma. NeuroImage: Clinical **12**, 34–40 (2016)
12. McNitt-Gray, M., et al.: Standardization in quantitative imaging: a multicenter comparison of radiomic features from different software packages on digital reference objects and patient data sets. Tomography **6**(2), 118 (2020)

13. Bakas, S., et al.: Overall survival prediction in glioblastoma patients using structural magnetic resonance imaging (MRI): advanced radiomic features may compensate for lack of advanced MRI modalities. J. Med. Imaging **7**(3), 031505 (2020)
14. Zwanenburg, A., et al.: The image biomarker standardization initiative: standardized quantitative radiomics for high-throughput image-based phenotyping. Radiology **295**(2), 328–338 (2020)
15. Bakas, S., et al.: In vivo detection of EGFRvlll in glioblastoma via perfusion magnetic resonance imaging signature consistent with deep peritumoral infiltration: the φ-index. Clin. Cancer Res. **23**(16), 4724–4734 (2017)
16. Binder, Z.A., et al.: Epidermal growth factor receptor extracellular domain mutations in glioblastoma present opportunities for clinical imaging and therapeutic development. Cancer Cell **34**(1), 163–177 (2018)
17. Akbari, H., et al.: In vivo evaluation of EGFRvlll mutation in primary glioblastoma patients via complex multiparametric MRI signature. Neuro Oncol. **20**(8), 1068–1079 (2018)
18. Bakas, S., et al.: GLISTRboost: combining multimodal MRI segmentation, registration, and biophysical tumor growth modeling with gradient boosting machines for glioma segmentation. In: Crimi, A., Menze, B., Maier, O., Reyes, M., Handels, H. (eds.) BrainLes 2015. LNCS, vol. 9556, pp. 144–155. Springer, Cham (2016). https://doi.org/10.1007/978-3-319-30858-6_13
19. Hogea, C., Davatzikos, C., Biros, G.: An image-driven parameter estimation problem for a reaction-diffusion glioma growth model with mass effects. J. Math. Biol. **56**(6), 793–825 (2008)
20. Ostrom, Q.T., et al.: Cbtrus statistical report: primary brain and central nervous system tumors diagnosed in the united states in 2008–2012. Neuro-oncology **17**(suppl_4), iv1–iv62 (2015)
21. Konukoglu, E., et al.: Image guided personalization of reaction-diffusion type tumor growth models using modified anisotropic eikonal equations. IEEE Trans. Med. Imaging **29**(1), 77–95 (2009)
22. Gooya, A., Biros, G., Davatzikos, C.: Deformable registration of glioma images using EM algorithm and diffusion reaction modeling. IEEE Trans. Med. Imaging **30**(2), 375–390 (2010)
23. Scheufele, K., Mang, A., Gholami, A., Davatzikos, C., Biros, G., Mehl, M.: Coupling brain-tumor biophysical models and diffeomorphic image registration. Comput. Methods Appl. Mech. Eng. **347**, 533–567 (2019)
24. Menze, B.H., et al.: A generative approach for image-based modeling of tumor growth. In: Székely, G., Hahn, H.K. (eds.) IPMI 2011. LNCS, vol. 6801, pp. 735–747. Springer, Heidelberg (2011). https://doi.org/10.1007/978-3-642-22092-0_60
25. Wang, C.H., et al.: Prognostic significance of growth kinetics in newly diagnosed glioblastomas revealed by combining serial imaging with a novel biomathematical model. Can. Res. **69**(23), 9133–9140 (2009)
26. Geremia, E., Menze, B.H., Prastawa, M., Weber, M.-A., Criminisi, A., Ayache, N.: Brain tumor cell density estimation from multi-modal MR images based on a synthetic tumor growth model. In: Menze, B.H., Langs, G., Lu, L., Montillo, A., Tu, Z., Criminisi, A. (eds.) MCV 2012. LNCS, vol. 7766, pp. 273–282. Springer, Heidelberg (2013). https://doi.org/10.1007/978-3-642-36620-8_27
27. Jackson, P.R., Juliano, J., Hawkins-Daarud, A., Rockne, R.C., Swanson, K.R.: Patient-specific mathematical neuro-oncology: using a simple proliferation and invasion tumor model to inform clinical practice. Bull. Math. Biol. **77**(5), 846–856 (2015)

28. Ivkovic, S., et al.: Direct inhibition of myosin ii effectively blocks glioma invasion in the presence of multiple motogens. Mol. Biol. Cell **23**(4), 533–542 (2012)
29. Wong, K.C., Summers, R.M., Kebebew, E., Yao, J.: Tumor growth prediction with reaction-diffusion and hyperelastic biomechanical model by physiological data fusion. Med. Image Anal. **25**(1), 72–85 (2015)
30. Clatz, O., et al.: Realistic simulation of the 3-D growth of brain tumors in MR images coupling diffusion with biomechanical deformation. IEEE Trans. Med. Imaging **24**(10), 1334–1346 (2005)
31. Rahman, M.M., Feng, Y., Yankeelov, T.E., Oden, J.T.: A fully coupled space-time multiscale modeling framework for predicting tumor growth. Comput. Methods Appl. Mech. Eng. **320**, 261–286 (2017)
32. Clark, K., et al.: The cancer imaging archive (TCIA): maintaining and operating a public information repository. J. Digit. Imaging **26**(6), 1045–1057 (2013)
33. Scarpace, L., et al.: Radiology data from the cancer genome atlas glioblastoma multiforme [TCGA-GBM] collection. Cancer Imaging Arch. **11**(4), 1 (2016)
34. Bakas, S., et al.: Segmentation labels and radiomic features for the pre-operative scans of the TCGA-GBM collection. The cancer imaging archive. Nat. Sci. Data **4**, 170117 (2017)
35. Cox, R., et al.: A (sort of) new image data format standard: Nifti-1: we 150. Neuroimage **22** (2004). https://nifti.nimh.nih.gov/nifti-1/documentation/hbm_nifti_2004.pdf
36. Menze, B.H., et al.: The multimodal brain tumor image segmentation benchmark (BRATS). IEEE Trans. Med. Imaging **34**(10), 1993–2024 (2014)
37. Bakas, S., et al.: Advancing the cancer genome atlas glioma MRI collections with expert segmentation labels and radiomic features. Scientific data **4**, 170117 (2017)
38. Bakas, S., et al.: Identifying the best machine learning algorithms for brain tumor segmentation, progression assessment, and overall survival prediction in the brats challenge. arXiv preprint arXiv:1811.02629 (2018)
39. Rohlfing, T., Zahr, N.M., Sullivan, E.V., Pfefferbaum, A.: The SRI24 multichannel atlas of normal adult human brain structure. Hum. Brain Mapp. **31**(5), 798–819 (2010)
40. Yushkevich, P.A., Pluta, J., Wang, H., Wisse, L.E., Das, S., Wolk, D.: Fast automatic segmentation of hippocampal subfields and medial temporal lobe subregions in 3 Tesla and 7 Tesla T2-weighted MRI. Alzheimer's Dementia **7**(12), P126–P127 (2016)
41. Yushkevich, P.A., et al.: User-guided 3D active contour segmentation of anatomical structures: significantly improved efficiency and reliability. Neuroimage **31**(3), 1116–1128 (2006)
42. Davatzikos, C., et al.: Cancer imaging phenomics toolkit: quantitative imaging analytics for precision diagnostics and predictive modeling of clinical outcome. J. Med. Imaging **5**(1), 011018 (2018)
43. Rathore, S., et al.: Brain cancer imaging phenomics toolkit (brain-CaPTk): an interactive platform for quantitative analysis of glioblastoma. In: Crimi, A., Bakas, S., Kuijf, H., Menze, B., Reyes, M. (eds.) BrainLes 2017. LNCS, vol. 10670, pp. 133–145. Springer, Cham (2018). https://doi.org/10.1007/978-3-319-75238-9_12
44. Pati, S., et al.: The cancer imaging phenomics toolkit (CaPTk): technical overview. In: Crimi, A., Bakas, S. (eds.) BrainLes 2019. LNCS, vol. 11993, pp. 380–394. Springer, Cham (2020). https://doi.org/10.1007/978-3-030-46643-5_38
45. Thakur, S., et al.: Brain extraction on MRI scans in presence of diffuse glioma: multi-institutional performance evaluation of deep learning methods and robust modality-agnostic training. NeuroImage **220**, 117081 (2020)

46. Allen, D.M.: The relationship between variable selection and data agumentation and a method for prediction. Technometrics **16**(1), 125–127 (1974)
47. Kather, J.N., et al.: Deep learning can predict microsatellite instability directly from histology in gastrointestinal cancer. Nat. Med. **25**(7), 1054–1056 (2019)
48. Kuo, C.-C., et al.: Automation of the kidney function prediction and classification through ultrasound-based kidney imaging using deep learning. NPJ Digit. Med. **2**(1), 1–9 (2019)
49. Student: Probable error of a correlation coefficient. Biometrika, pp. 302–310 (1908)
50. Mang, A., et al.: SIBIA-GLS: scalable biophysics-based image analysis for glioma segmentation. In: The Multimodal Brain Tumor Image Segmentation Benchmark (BRATS), MICCAI (2017)